Impact of Tidal Mixing on Water Mass Transformation and Circulation in the South China Sea

XIAOWEI WANG

State Key Laboratory of Tropical Oceanography, South China Sea Institute of Oceanology, Chinese Academy of Sciences, Guangzhou, China

ZHIYU LIU

State Key Laboratory of Marine Environmental Science, and Department of Physical Oceanography, College of Ocean and Earth Sciences, Xiamen University, Xiamen, China

SHIQIU PENG

State Key Laboratory of Tropical Oceanography, South China Sea Institute of Oceanology, Chinese Academy of Sciences, Guangzhou, and Laboratory for Regional Oceanography and Numerical Modeling, Qingdao National Laboratory for Marine Science and Technology, Qingdao, China

(Manuscript received 24 July 2016, in final form 1 December 2016)

ABSTRACT

Using a high-resolution regional ocean model, the impact of tidal mixing on water mass transformation and circulation in the South China Sea (SCS) is investigated through a set of numerical experiments with different configurations of tide-induced diapycnal diffusivity. The results show that including tidal mixing in both the Luzon Strait (LS) and SCS has significant impact on the LS transport and the intermediate–deep layer circulation in the SCS Basin. Analysis of the density field indicates that tidal mixing in both the LS and SCS are essential for sustaining a consistent density gradient and thus a persistent outward-directed baroclinic pressure gradient both between the western Pacific and LS and between the LS and SCS Basin, so as to maintain the strong deep-water transport through the LS. Further analysis of water mass properties suggests that tidal mixing in the deep SCS would strengthen the horizontal density gradient, intensify the basin-scale cyclonic circulation, induce more vigorous overturning, as well as generate the subbasin-scale eddies in the abyssal SCS. The results imply that tidal mixing in both the LS and SCS plays a key dynamic role in controlling water mass properties and deep circulation features in the SCS and thus need to be deliberately parameterized in ocean circulation models for this region.

1. Introduction

Diapycnal turbulent mixing is identified as one of the most important controlling factors of many physical and dynamic processes in the world's oceans. The global ocean stratification and meridional overturning circulation (MOC) are largely sustained by diapycnal mixing (Marshall and Speer 2012; Talley 2013). Observed diapycnal diffusivity ranges from $O(10^{-5})\,\mathrm{m^2\,s^{-1}}$ in the ocean interior far from boundaries (Ledwell et al. 1993) to greater than $O(10^{-3})\,\mathrm{m^2\,s^{-1}}$ over regions of rough topography, such as seamounts, ridges, canyons (e.g., Polzin et al. 1997; Ledwell et al. 2000; Carter and Gregg 2002), and continental shelves in marginal seas (e.g., MacKinnon and Gregg 2003). To sustain the diapycnal mixing, there must be a continuous supply of mechanical energy (Huang 1999; MacKinnon 2013). Wunsch and Ferrari (2004) postulated that the energy of near-inertial waves generated by surface wind is dissipated mostly within the upper ocean; however, how deep the wind energy input can penetrate is still up for debate (Alford et al. 2012; Wu et al. 2011). The global energy of internal lee waves generated by quasi-steady flow and mesoscale eddies over rough topography is estimated to be about 0.2–0.4 TW (Nikurashin and Ferrari 2013; Scott et al. 2011). Another energy source for diapycnal mixing is the internal tides generated by the interaction of barotropic

Corresponding author e-mail: Shiqiu Peng, speng@scsio.ac.cn

DOI: 10.1175/JPO-D-16-0171.1

tides with rough topography. The global energy conversion from barotropic tides to internal tides in the deep ocean is estimated to be around 1 TW (Egbert and Ray 2000; Jayne and St. Laurent 2001; Niwa and Hibiya 2014), about half of the 2 TW required to maintain the global MOC (Munk and Wunsch 1998). Therefore, tidal mixing dominates among these factors that contribute to the diapycnal mixing in the global deep ocean, in particular in the South China Sea (SCS) where enormously energetic internal tides are known to be generated in the Luzon Strait (LS; Alford et al. 2015; Ma et al. 2013; Zhao 2014).

A semiempirical parameterization scheme for tidal mixing was proposed by St. Laurent et al. (2002, hereinafter referred to as LSJ02), which represents local dissipation of internal tides, that is, the dissipation of internal tides near their generation sites, with magnitude of local barotropic tidal currents, roughness of bottom topography, and bottom stratification (Jayne and St. Laurent 2001). The LSJ02 parameterization has been implemented in several global ocean general circulation models in the recent decade. Simmons et al. (2004) carried out the first application of this mixing scheme in a coarse-resolution model of the global ocean, and their climatological comparisons show a substantial reduction of temperature T and salinity S biases using the parameterization compared to the cases using either a globally constant value or the Bryan and Lewis (1979) formulation. The experiments of Saenko and Merryfield (2005) suggested that the enhanced diapycnal mixing due to internal tides increases bottom-water circulation and deep stratification, significantly intensifies and deepens the Antarctic Circumpolar Current (ACC), and increases bottom-water formation around Antarctica. Jayne (2009) compared simulations with various parameter choices and found that LSJ02 has a noticeable impact on the simulated global MOC and the transport of the ACC. Melet et al. (2013) compared two simulations employing the LSJ02 and Polzin (2009) parameterization, respectively, and found that the global ocean state is sensitive to the vertical profile of tidal mixing.

There are, however, very few studies conducted on the marginal seas, as compared to the open ocean. Koch-Larrouy et al. (2007, 2008a,b) applied a modified LSJ02 scheme in a regional model of the Indonesian Seas to investigate the effect of tidal mixing on water mass transformation along the Indonesian Throughflow and in the equatorial current system. They found that tidal mixing has predominant impact on the T–S characteristics of the Banda Sea and the Indonesian Throughflow (Koch-Larrouy et al. 2007). They also found that internal tides are the only energy source for creating the thermocline water and the Indonesian outflow water and make seawater absorb more heat from the atmosphere by cooling the surface water (Koch-Larrouy et al. 2008b). The model with parameterization of tidal mixing can reproduce the observed salty water penetration from the subtropical South Pacific, the thermocline stratification in the southern Indonesian basins, and the cold and fresh tongue exiting into the Indian Ocean (Koch-Larrouy et al. 2008a).

The SCS is a semienclosed marginal sea located in the northwest Pacific Ocean (PO), with the LS being the only deep-water passage connecting the SCS to the PO. The Bashi Channel with a depth of about 2400 m is the deepest connection in the LS. Thus, below 2400 m, the SCS is an isolated basin without direct water exchange with surrounding oceans. However, the colder and denser Pacific Water can sink into the SCS Basin below 2400 m after it crosses the LS; thus, net upwelling must occur in the deep SCS to compensate the overflow (Qu et al. 2006). The upper circulation in the SCS driven mainly by the seasonally reversing monsoon has been investigated extensively over the past several decades, which is subject to a significant seasonal variation with generally a cyclonic circulation in winter and an anticyclonic circulation in summer (e.g., Wyrtki 1961; Chu et al. 1999; Shaw and Fu 1999; Chu and Li 2000; Qu 2000; Liu et al. 2001; Xue et al. 2004; Fang et al. 2009). In contrast, there are very few studies on the intermediate and deep circulations. Analysis of the thermohaline structure, dissolved oxygen, and sediment distributions in the SCS reveals the existence of a basin-scale anticyclonic circulation in the intermediate layer and a cyclonic circulation in the deep layer (Yuan 2002; Li and Qu 2006; Qu et al. 2006; Wang et al. 2011; Lan et al. 2013, 2015; Gan et al. 2016), accompanied by a "sandwich" structure of the SCS overturning circulation as envisioned from the high-resolution global reanalysis data (Shu et al. 2014). Because of the lack of sufficient observations, the detailed structures of water properties and circulation in the intermediate and deep SCS remain largely unknown.

The basin-averaged diapycnal diffusivity in the SCS required to reproduce the observed water mass transformation is estimated to be $10^{-3}\,\mathrm{m^2\,s^{-1}}$ based on a 1D advection–diffusion model (Qu et al. 2006). Elevated diapycnal mixing due to the enormous energy dissipation of internal tides in the LS and SCS, with a maximum up to $10^{-2}\,\mathrm{m^2\,s^{-1}}$, are reported (St. Laurent 2008; Tian et al. 2009; St. Laurent et al. 2011; Liu and Lozovatsky 2012; Lozovatsky et al. 2013; Yang et al. 2014, 2016; Wang et al. 2016). It has been speculated that diapycnal mixing is the primary driving force of the deep-water transformation and overturning circulation in the LS and

SCS region. The North Pacific Deep Water (NPDW; Mantyla 1975) overflows through the LS in the deep layer (Tian et al. 2006; Chang et al. 2010) and gradually gets mixed by strong turbulence generated by the dissipation of internal tides (Tian et al. 2009), which maintains the baroclinic pressure gradient across the LS as well as drives the deep transport through the LS (Zhao et al. 2014) and a basin-scale upwelling in the deep SCS (Qu et al. 2006). The NPDW eventually leaves the SCS for the PO and surrounding seas through the LS in the intermediate layer (Chao et al. 1996; Chen and Huang 1996; Tian et al. 2006; Gan et al. 2016) and through the Taiwan, Mindoro, and Karimata Straits in the upper layer (Qu et al. 2009; Yaremchuk et al. 2009). Nevertheless, some important issues on the connection between the intermediate and deep circulation in the SCS and tidal mixing in the LS and SCS remain open, such as whether the tidal mixing contributes to the formation of the subbasin-scale deep circulation, to what extent tidal mixing determines the overturning circulation as well as the deep-water renewal of the basin, and what the individual, dynamic role of the tidal mixing in the LS and the SCS, respectively, is in water transformation and circulation.

The purpose of this paper is to investigate the impact of tidal mixing on the circulation and water properties in the SCS through a set of numerical experiments with different mixing schemes employed in a high-resolution regional model. We implemented the tidal mixing scheme devised by Wang et al. (2016), which is based on energetics of internal tides and can thus represent enhanced diapycnal mixing induced by dissipation of internal tides generated both locally and remotely. Note, however, that possible reductions of model biases or reproduction of observed features will not be our focus when using different mixing schemes because 1) impacts on model biases would be model dependent (Melet et al. 2013) and 2) observations in the deep water available for model validation are very limited. Instead, this study explores sensitivity of the ocean state to tidal mixing in the LS and SCS regions and the relevant dynamic mechanisms, which are not expected to depend on detailed model configurations.

The rest of this paper is organized as follows: The parameterization scheme of tidal mixing is described in section 2. The model configuration and numerical experiments are introduced in section 3. Section 4 presents the results of the numerical experiments, which are then discussed and summarized in section 5.

2. Tidal mixing parameterization

Our tidal mixing scheme in the LS and SCS regions follows the work of Wang et al. (2016). The generation and radiation of internal tides are simulated by a three-dimensional, high-resolution, internal tide model, with both the local and remote dissipation of internal tides being implicitly resolved. The depth-integrated dissipation rate of baroclinic energy $\langle \mathrm{DIS_{bc}} \rangle$ is calculated as the difference of the divergence of the depth-integrated baroclinic energy flux $\mathbf{F}_{\mathrm{bc}}$ and the depth-integrated barotropic-to-baroclinic energy conversion rates E_{bt2bc}:

$$\langle \mathrm{DIS_{bc}} \rangle \approx -\langle E_{\mathrm{bt2bc}} \rangle + \langle \nabla_h \cdot \mathbf{F}_{\mathrm{bc}} \rangle , \tag{1}$$

where

$$\nabla_h \cdot \mathbf{F}_{\mathrm{bc}} = \nabla_h \cdot \left(\int_{-H}^{\eta} \mathbf{u}' p' \, dz \right), \quad \text{and} \tag{2}$$

$$E_{\mathrm{bt2bc}} = g \int_{-H}^{\eta} \rho' w_{\mathrm{bt}} \, dz , \tag{3}$$

and the angle brackets represent tidal averaging. The variables H and η denote the time-mean water depth and surface tidal elevation, respectively; w_{bt} is the vertical velocity associated with barotropic tides; ρ' and p' are the perturbations of density and pressure, respectively; and $\mathbf{u}'$ is the baroclinic velocity. These quantities are all estimated from the tidal simulation of Wang et al. (2016), to which we refer for a detailed introduction to the methodology.

In principle, a 3D analysis of internal tide energetics is possible with model-simulated quantities, but the results are very sensitive to the mixing scheme and other aspects of dynamics in the tidal model. To avoid uncertainties in calculating the vertical energy transport, we examine the depth-integrated baroclinic energy budget [Eq. (1)] based on the depth-integrated baroclinic energy equation.

Since the baroclinic energy budget analysis can only produce a 2D rather than 3D distribution of energy dissipation, a known/assumed vertical structure function of the tidal energy dissipation is needed to obtain a 3D tidal mixing estimate. Unfortunately, because of the lack of substantial microstructure observations, the vertical distribution of tidal dissipation remains unknown. To proceed, we adopt the vertical structure function $F(z)$ in the LSJ02 parameterization formulated as

$$F(z) = \frac{\exp[-(D+z)/\zeta]}{\zeta[1-\exp(-D/\zeta)]}, \tag{4}$$

assuming that both the local and remote tidal dissipations are bottom intensified and exponentially decay away from the seafloor. Here, ζ is the vertical decay scale taken to be $\zeta = 500$ m, according to LSJ02, and D is the total water depth.

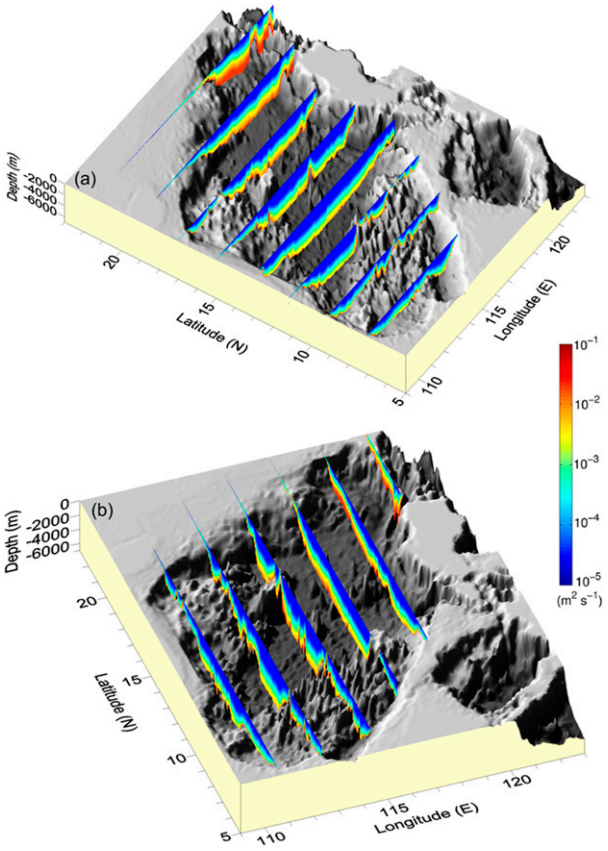

FIG. 1. The spatial distributions of the tide-induced diapycnal diffusivity estimated from internal tide energetics along the (a) zonal sections (every 2° latitude between 7° and 21°N) and (b) meridional sections (every 2° longitude between 111° and 121°E).

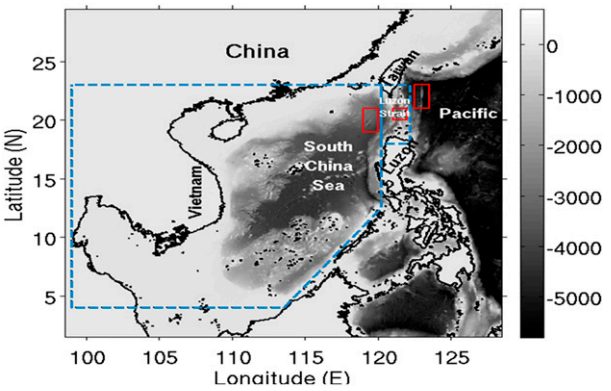

FIG. 2. Bathymetry of the model domain. The two blue dashed boxes bound the areas of the SCS and of the LS, respectively. The three red boxes indicate the areas of PO (21° to 23°N, 122.5° to 123.5°E), LS (20° to 21°N, 121° to 122°E), and SCS (19° to 21°N, 119° to 120°E), respectively, used to calculate area-averaged potential density profiles.

Thus, the diapycnal diffusivity induced by the dissipation of locally and remotely generated internal tides is calculated by

$$\kappa_v = \frac{\Gamma \langle \mathrm{DIS_{bc}} \rangle F(z)}{\rho N^2} + \kappa_0. \tag{5}$$

Here, Γ is the mixing efficiency, set to be 0.2 according to Osborn (1980), κ_0 is the background diffusivity and is specified as $\kappa_0 = 1 \times 10^{-5}\,\mathrm{m^2\,s^{-1}}$, and ρ and N^2 are the seawater density and the squared buoyancy frequency, respectively. Therefore, the scheme is similar to LSJ02 except that it takes into account the dissipation of remotely generated internal tides besides the local tidal dissipation. It is more realistic and thus more accurate in representing tidal mixing in the SCS, where the major source of turbulent kinetic energy is internal tides generated in the LS radiating into the entire SCS Basin.

The estimated diapycnal diffusivity is subject to significant spatial variability throughout the LS and SCS region (Fig. 1). The strongest tidal mixing occurs in the LS and the northern SCS Basin. In the LS, the diapycnal diffusivity is of $O(10^{-2})\,\mathrm{m^2\,s^{-1}}$ atop the two ridges. In the SCS, the diapycnal diffusivity is of $O(10^{-4}$–$10^{-3})\,\mathrm{m^2\,s^{-1}}$ in the continental shelfbreak region and of $O(10^{-3}$–$10^{-1})\,\mathrm{m^2\,s^{-1}}$ in the deep water. As shown in Wang et al. (2016), these results are generally consistent with diapycnal diffusivity estimates from turbulence microstructure measurements and finescale parameterizations. Therefore, this tidal mixing scheme is suitable for exploring the impact of tidal mixing on the water mass transformation and circulation in the SCS.

3. Model configurations

The regional model used in this study is based on the Massachusetts Institute of Technology General Circulation Model (MITgcm; Marshall et al. 1997). The model is structured in z coordinates, and the Gent–McWilliams/Redi subgrid-scale (SGS) eddy parameterization (GMRedi parameterization) is adopted to eliminate spurious diapycnal mixing introduced by advection schemes. The GMRedi parameterization mixes tracer properties along isopycnal surfaces by orienting the diffusion tensor into the isopycnal and diapycnal directions (Redi 1982) and adiabatically rearranges tracers through an advective flux (Gent and McWilliams 1990; Gent et al. 1995).

Our model domain extends from 2° to 29°N in latitude and from 98.5° to 128.5°E in longitude, including the entire SCS Basin, the LS region, as well as part of the northwest Pacific Ocean (Fig. 2). The model has a high resolution of 1/12° × 1/12° in the horizontal direction and 60 z levels in the vertical. The thickness of layers

gradually increases from 10 to 50 m within the 0–300-m water depth, 100 m within 300–4500-m water depth, and 200 m below 4500-m water depth.

The mixing parameterization is set as follows: The horizontal and vertical eddy viscosities are calculated with the Smagorinsky (1993) scheme and the KPP scheme (Large et al. 1994), respectively. The isopycnal diffusivity is set to be $500\,m^2\,s^{-1}$. Different configurations of the diapycnal diffusivity estimated from the parameterization specified in section 2 are adopted in different numerical experiments as detailed below. Note that the actual distribution of isopycnal and diapycnal mixing in the model is somehow different from what we specified because the model is based on z coordinates and the GMRedi scheme is applied to orientate the diffusion tensor into the isopycnal and diapycnal directions.

We carried out four numerical experiments. The experiment NoTM is configured with the standard KPP scheme with a uniform background diffusivity of $1 \times 10^{-5}\,m^2\,s^{-1}$, which is the only run without consideration of tidal mixing. The other three experiments are configured with modified KPP schemes, that is, replacing the constant background value in the KPP scheme with different considerations of tidal mixing. In the experiments TM-LS and TM-SCS, tidal mixing solely in the LS and the SCS region, respectively, is considered in order to isolate the individual impact of tidal mixing in the two regions (Fig. 2). In experiment TM-SCSLS, tidal mixing in both the LS and the SCS regions is considered.

The model topography is taken from the General Bathymetric Chart of the Oceans (GEBCO_08) bathymetry data (http://www.gebco.net/) with a high resolution of 30 arc s. The initial temperature and salinity fields are the monthly mean of January derived from the Generalized Digital Environmental Model, version 3 (GDEMv3), climatology (http://www.usgodae.org/pub/outgoing/static/ocn/gdem/). The model is forced by the climatological monthly mean wind stress calculated from the cross-calibrated multiplatform (CCMP) datasets (Atlas et al. 2011) with a relaxation of the sea surface temperature and salinity to the monthly mean GDEMv3 climatology. In the three (northern, southern, and eastern) open boundaries, where a sponge layer is assumed, the model thermodynamic variables are also relaxed to the climatology.

All the numerical experiments start from an initial state of rest and run for 100 yr. As shown in Fig. 3, the total kinetic energy of both the upper (0–2000 m) and deep (2000–bottom) SCS reaches quasi equilibrium by the end of the 100-yr simulation for all experiments, and the experiment TM-SCSLS takes the least time of about 20 yr to achieve its equilibrium state for the deep SCS. We therefore take the annual mean of the 100th model year for further analysis. Note that since the tide-induced diapycnal diffusivity considered in the experiments is an annual mean without seasonal evolution, the seasonal cycle features of circulation and water mass transformation in the SCS are not considered in this study. Note also that although it may be more reasonable to conduct the analyses on isopycnal surfaces along which the water moves approximately, we conduct the analysis on isobath surfaces in this study to avoid potential errors induced by the coordinate transformation from isobath surfaces of the z-coordinate model to isopycnal surfaces and to ensure everything is self-consistent within the dynamic framework of the model. The same analysis has in fact been conducted in many previous studies (Huang and Jin 2002; Saenko and Merryfield 2005; Jayne 2009). This makes it easier to compare our results with the existing studies.

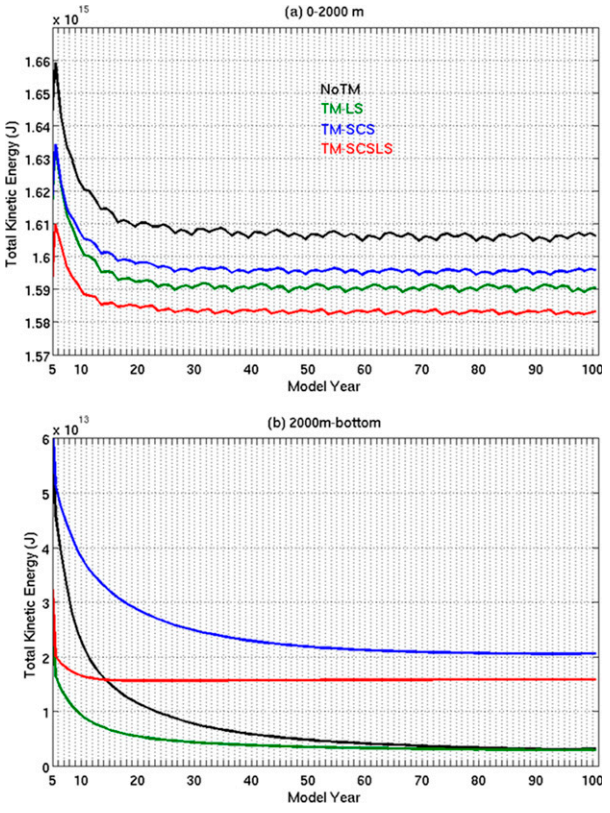

FIG. 3. Time evolution of annual-mean total kinetic energy over the SCS region in the layers of (a) 0–2000- and (b) 2000-m bottom for different experiments.

4. Results

a. *Water mass properties*

The basin-averaged differences of potential temperature θ and salinity S in the SCS between the experiments including tidal mixing and the experiment NoTM

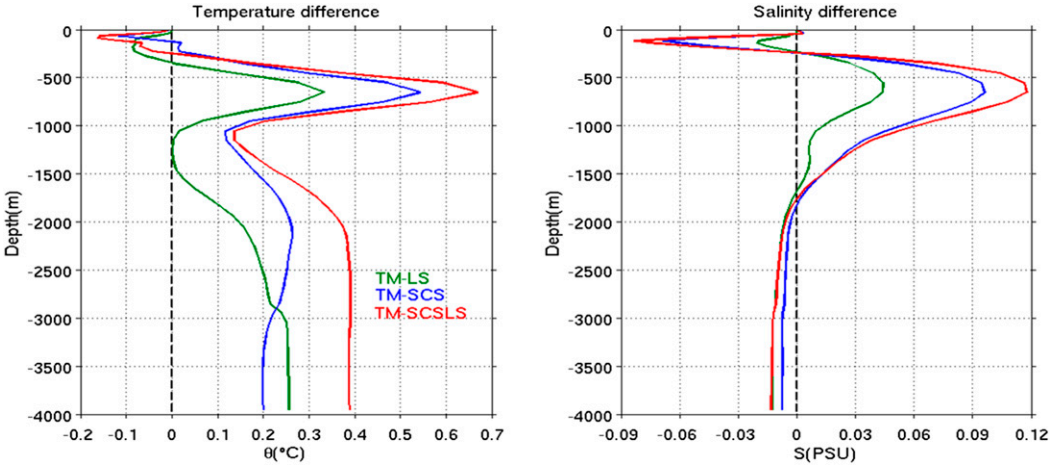

FIG. 4. Basin-averaged differences of potential temperature θ and salinity S in the SCS between the experiments with tidal mixing and the experiment NoTM.

are shown in Fig. 4. The simulated water mass properties at the same layer show similar qualitative differences in all the experiments with tidal mixing. Under the influence of tide-induced diapycnal mixing, the water masses become colder and fresher in the subsurface layer, warmer and saltier in the intermediate layer, and warmer and fresher in the deep layer. The largest differences appear in TM-SCSLS with elevated diapycnal diffusivity in both the LS and SCS, suggesting that the deep water is significantly lightened with the warmer and fresher water overlying through tidal mixing. Taking TM-SCSLS, for example, the cross-section distributions of θ and S differences along 17°N and 115°E are shown in Fig. 5, respectively. Although diapycnal mixing is locally elevated over the continental slope, seamounts, and abyssal basin (Wang et al. 2016), the water mass

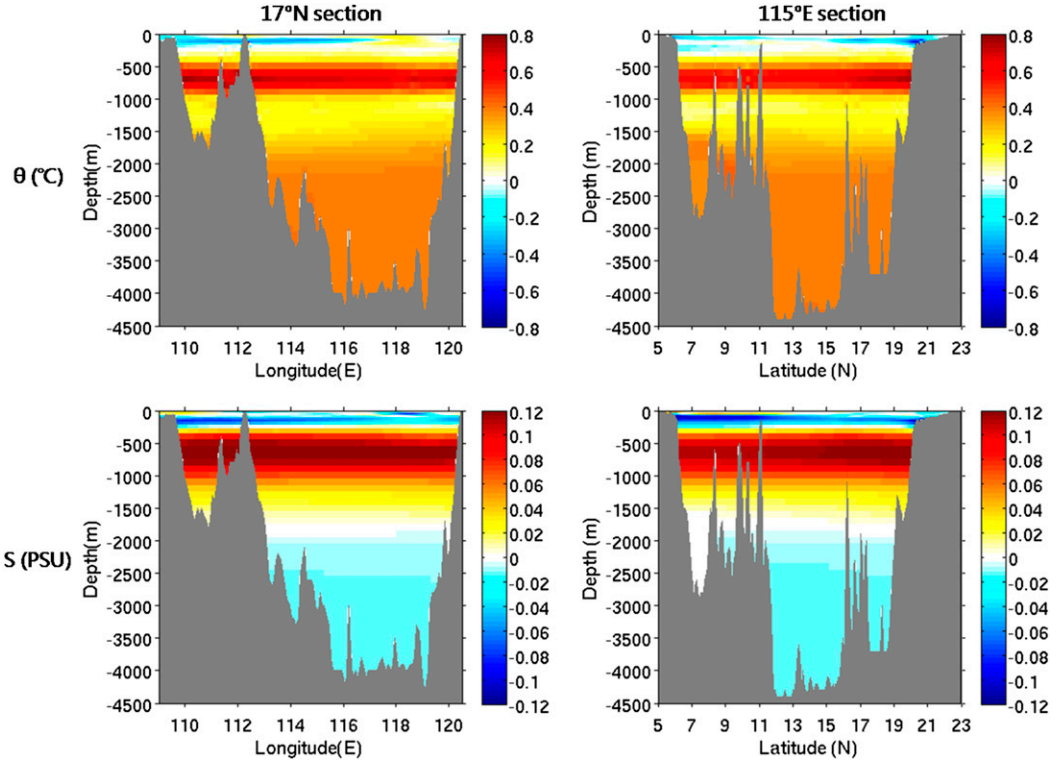

FIG. 5. Cross-section distributions of the differences in potential temperature θ and salinity S between TM-SCSLS and NoTM, along 17°N and 115°E, respectively.

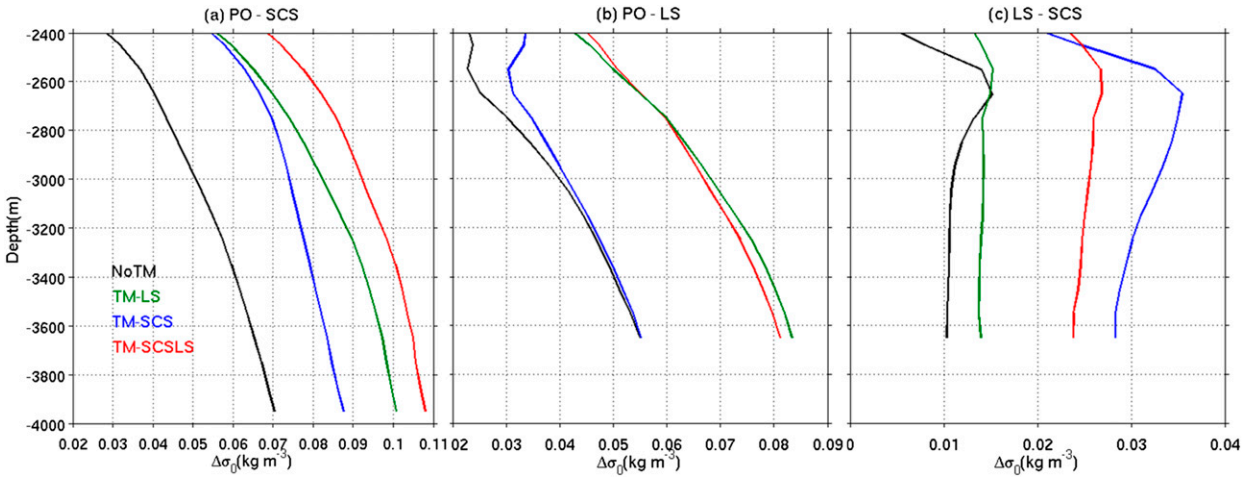

FIG. 6. Vertical profiles of potential density differences $\Delta\sigma_0$ below 2400 m between (a) the PO and SCS, (b) the PO and LS, as well as (c) the LS and SCS for different experiments. The bounds of the three areas are marked with three red boxes in Fig. 2.

properties within the same layer over the whole basin show almost identical variation, with relatively larger changes where the diapycnal diffusivity is bigger. These results suggest that tidal mixing enhances the SCS water transformation at the basin scale.

The area-averaged density profiles within and on both sides of the LS below 2400 m are used to examine the horizontal density differences of the deep water between any two regions of the PO, LS, and SCS (Fig. 6). The horizontal pressure gradient at a certain depth is proportional to the gradient of the depth integration of the density anomaly from the sea surface down to that depth. According to the simplified hydraulic theory of Qu et al. (2006), we can consider the water overlying the deep water as a layer of motionless fluid with slightly lower density; thereby, the potential density gradient of the deep water can be taken as a proxy of the horizontal baroclinic pressure gradient relative to the overlying water. Among all experiments, NoTM shows the lowest density differences between any two regions. For experiments with tidal mixing, the density difference in TM-LS is the highest between the PO and LS (Fig. 6b), but the lowest between the LS and SCS (Fig. 6c), whereas that in TM-SCS shows a completely opposite result. As expected, the density difference in TM-SCSLS keeps relatively high between the adjacent regions and becomes the highest between the PO and SCS (Fig. 6a). These comparisons reveal that tidal mixing in a sole region of the LS or the SCS can only sustain the density gradient between the upstream and the local region, while tidal mixing in both the LS and SCS are necessary to maintain a consistent density gradient across the LS and thus provide an outward-directed baroclinic pressure gradient relative to the overlying water.

To further examine properties of deep water, Fig. 7 shows the horizontal maps of potential density σ_0 at 3000 m in the SCS Basin. In NoTM (Fig. 7a), relatively high σ_0 is along the northern and western continental margins, and the low value is in the southeastern part of the SCS, with about 27.697 kg m^{-3} to the west of the LS and about 27.695 kg m^{-3} in the southeastern corner of the basin. In TM-LS (Fig. 7b), because of the highest level of diapycnal diffusivity applied in the LS, the NPDW gets strongly mixed with the overlying light water within the LS; thus, it leads to a much lower σ_0 (about 27.665 kg m^{-3}) water intrusion into the deep SCS, and the low σ_0 water stays rather uniform in the whole SCS Basin, only decreasing slightly by less than 0.002 kg m^{-3} between the LS vicinity and the southeastern corner of SCS. In TM-SCS (Fig. 7c), with the tide-induced diapycnal mixing in the SCS, σ_0 is lower/higher than that in NoTM/TM-LS and the horizontal gradients of σ_0 in the whole SCS deep basin strengthen extremely, especially around the LS vicinity and the central seamounts in the northern basin, the western boundary, and the southeastern corner in the southern basin. In TM-SCSLS (Fig. 7d), σ_0 has generally the same pattern but relatively lower horizontal gradient than that in TM-SCS, and the value of σ_0 is the lowest among all experiment due to the effect of tidal mixing in the LS as shown in TM-LS (Fig. 7b).

The simulated patterns of potential density in TM-SCS and TM-SCSLS show a good agreement with previous reports based on hydrographic data and dissolved oxygen concentration from the World Ocean Database (Qu 2002; Qu et al. 2006) but are different from the GDEMv3 data, which have a light-water core west of Luzon Island (Wang et al. 2011). These results indicate

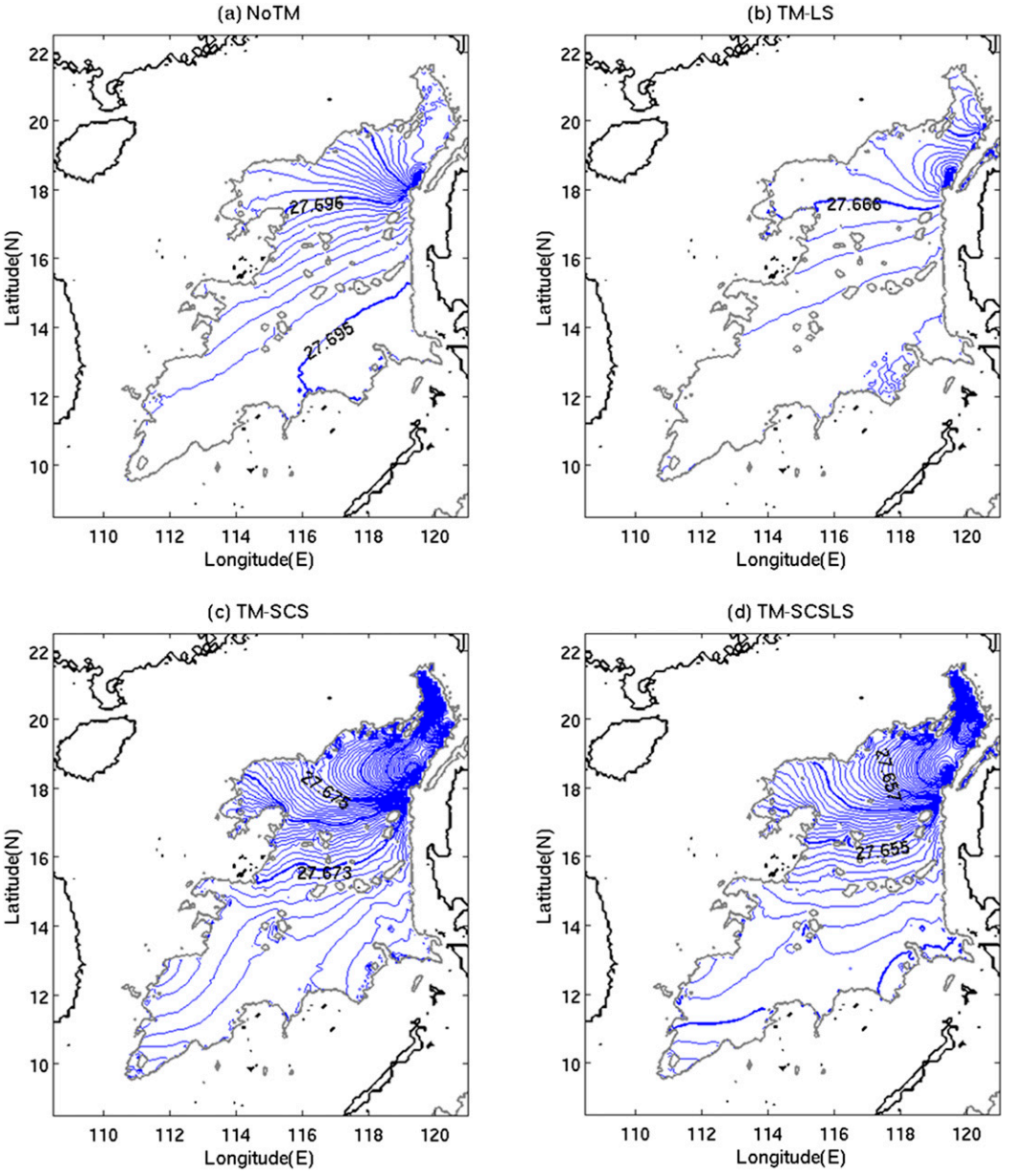

FIG. 7. Potential density σ_0 (kg m^{-3}) at 3000 m in the SCS for the experiment (a) NoTM, (b) TM-LS, (c) TM-SCS, and (d) TM-SCSLS. The blue contours intervals are 0.0001 kg m^{-3}. The gray contours represent the 3000-m isobaths.

that tidal mixing in the deep LS would make the intruded water too light and weaken the horizontal density difference within the SCS Basin, while tidal mixing in the deep SCS would maintain and strengthen the horizontal density gradient in the SCS Basin.

b. Luzon Strait transport

The water fluxes across 121°E in the layers of 0–500 m, 500–1000 m, and from 1500 m to bottom are calculated as the transports in the upper, intermediate, and deep layers in the LS, respectively. Figure 8 shows the transport evolutions of the four experiments. The transport in the upper layer appears to be only weakly impacted by tidal mixing (Fig. 8a), with the differences between any two experiments of less than 0.20 Sv (1 Sv $\equiv 10^6$ m^3 s^{-1}), while the transports in the intermediate and deep layers are both significantly impacted by tidal mixing. In the intermediate layer (Fig. 8b), the annual mean transport without tidal mixing (NoTM) decreases continuously after spinup and shifts from outflow to inflow after about

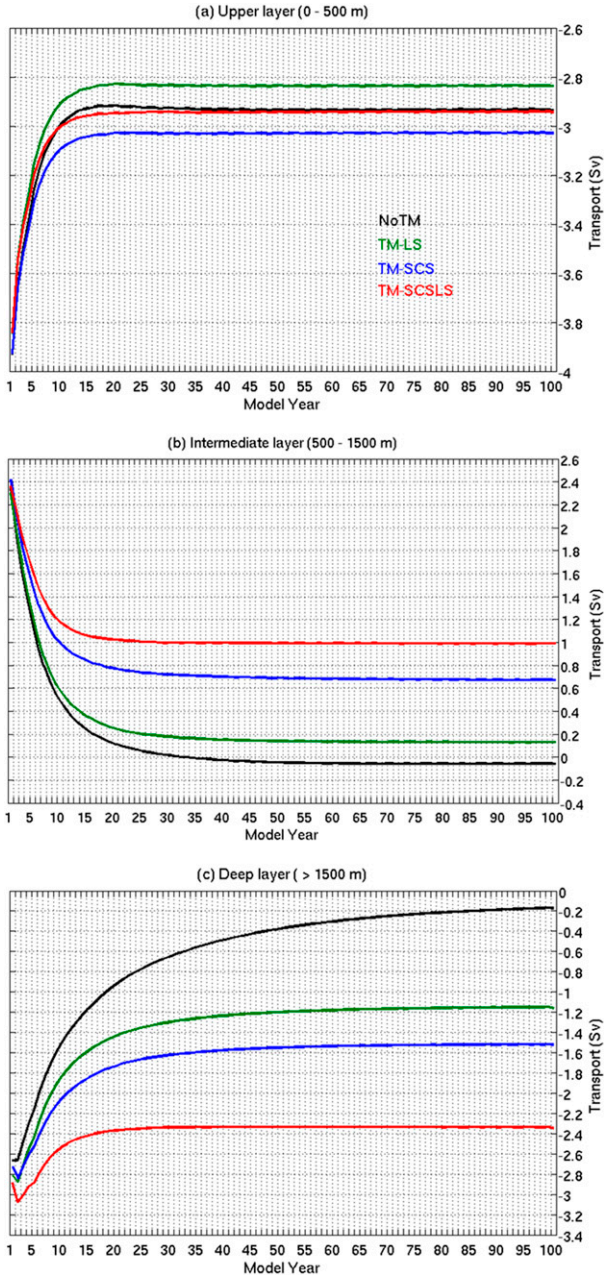

FIG. 8. Time evolution of annual mean transports through the LS in the (a) upper, (b) intermediate, and (c) deep layers for different experiments.

50 yr of integration. In the other three experiments with tidal mixing (i.e., TM-LS, TM-SCS, and TM-SCSLS), the decrease of transport during model spinup all weakens with the transport, eventually reaching an equilibrium state of about 0.13, 0.68, and 1.0 Sv, respectively, in the 100th model year. The largest value (1.0 Sv) obtained in TM-SCSLS is more consistent with the results from high-resolution global reanalysis data (Xie et al. 2013; Shu et al. 2014). The results suggest that tide-induced diapycnal mixing in both the LS and SCS is essential in driving the water transport in the intermediate layer through the LS.

In the deep layer (Fig. 8c), the annual-mean transport of NoTM decreases rapidly after spinup and remains variable in the 100th model year with a value of 0.17 Sv. In contrast, the annual-mean deep transports in TM-LS, TM-SCS, and TM-SCSLS all reach quasi-equilibriums by the 100th model year, with a value of about 1.16, 1.52, and 2.35 Sv, respectively. In previous studies, the estimated mean transport of deep-water overflow through the LS ranges from 0.5 to 2.5 Sv, based on diagnostic calculations (e.g., Wang 1986; Qu et al. 2006), instantaneous hydrographic data (e.g., Tian et al. 2006; Yang et al. 2010), and mooring observations (Liu and Liu 1988; Chang et al. 2010; Zhou et al. 2014), as well as numerical simulations (Zhao et al. 2014). The present estimate in TM-SCSLS is close to the upper bound of these estimates. Given the deep-water transport in the LS and the total volume below 1500 m in the SCS (about 1.9×10^{15} m^3; Qu et al. 2006), the residence time of the SCS deep water in TM-LS, TM-SCS, and TM-SCSLS is estimated to be roughly 52, 40, and 26 yr, respectively, as compared to 24 yr estimated by Qu et al. (2006). Therefore, the tide-induced diapycnal mixing in the LS or/and SCS significantly speeds up the deep-water renewal in the SCS Basin.

Previous diagnostic estimates of the deep-water transport through the LS are generally based on the density difference between the PO and SCS, and the hydraulic theory with assumptions of flat bottom in the LS (e.g., Qu et al. 2006). However, our experiments show that the strength of transport is not exactly consistent with the density difference between the PO and SCS (Fig. 6a) or that between the adjacent regions (Figs. 6b,c). This is because the section used to estimate the transport is set between the LS and the SCS, as done in most previous studies. The tidal mixing solely in the LS cannot sustain relatively high density gradient between the LS and SCS but that in the SCS can (Fig. 6c), so the deep-water transport in TM-SCS is relatively higher than that in TM-LS. This is probably why most previous studies only emphasize the enhanced diapycnal mixing in the SCS and recognize it as a key process responsible for the density difference between the PO and SCS, which drives the deep-water transport through the LS (e.g., Zhao et al. 2014). Nevertheless, our experiments indicate that, besides tidal mixing in the SCS, tidal mixing in the LS also plays an important role in sustaining the density gradient between the PO and LS as well as between the PO and SCS (Figs. 6b,a); thus, the impact of tidal mixing in the LS must be taken into

account in the simulation of deep-water mass transformation and transport through the LS.

In NoTM, TM-LS, and TM-SCS, relatively weaker diapycnal mixing in either the SCS (for TM-LS) or the LS (for TM-SCS) or both (for NoTM) cannot sustain the consistent high density gradient through the LS, and thus the horizontal pressure gradient that drives the deep-water overflow between the PO and the SCS weakens gradually. As a result, the deep transport in NoTM decreases continuously and probably vanishes after sufficiently long model integration, and the deep transports in TM-LS and TM-SCS are much weaker than that in TM-SCSLS. In contrast, the deep-water transport in TM-SCSLS can reach an equilibrium state with a high value because tide-induced diapycnal mixing in both the LS and SCS can maintain the consistent water mass transformation and thus the required horizontal pressure gradient force through the LS (e.g., Qu et al. 2006). The results of our experiments reveal that tidal mixing in both the LS and SCS is necessary to sustain the deep-water transport through the LS.

c. Deep circulation

Figure 9 shows the vertical-averaged currents from 2400 m to the bottom in the SCS Basin for all the experiments. In NoTM (Fig. 9a), there is a predominant basin-scale cyclonic circulation around the seamounts in the central SCS with a narrow deep western boundary current. In TM-LS (Fig. 9b), the boundary current and the cyclonic circulation weaken dramatically throughout the entire basin, as a result of the decreased horizontal density gradients in the SCS Basin (Fig. 7b), suggesting that the tide-induced diapycnal mixing in the LS would have a negative effect on driving the cyclonic deep circulation in the SCS.

In contrast, the simulated cyclonic deep circulation in the SCS is significantly enhanced in TM-SCS (Fig. 9c) with three subbasin-scale cyclonic eddies embedded (indicated by the dashed circles in Fig. 9c). It can be seen that the NPDW, after entering the SCS through the LS, flows southward along the continental margins off southeast China and east Vietnam as a stronger, west-intensified boundary current and extends to the southwestern corner of the SCS deep basin before being mixed away in the basin interior. The intrusion of NPDW and the basin-scale cyclonic gyre are consistent with the existence of lower potential temperature and higher potential density near the western boundary than in the central basin (Qu et al. 2006) as well as with the distribution of the oxygen concentration in the SCS (Qu 2002). The multieddies in the interior of the SCS Basin are similar, though with much smaller velocities, to those identified from the deep geostrophic current calculation using the GDEM data (Wang et al. 2011). The results in TM-SCSLS (Fig. 9d) are quite similar to those in TM-SCS, with relatively smaller velocities due to the relatively weaker density gradient under the effect of tidal mixing in the LS (Figs. 7c,d).

Previous studies attribute the abyssal cyclonic circulation to the drive by the Luzon overflow (Lan et al. 2013, 2015) and the constraint of topographic effects (Qu et al. 2006; Wang et al. 2011). The results of our experiments reveal that tide-induced diapycnal mixing in the LS and SCS has significant impact on both the deep LS transport and the basin-scale deep circulation in the SCS. Moreover, it is possible that the bottom-intensified tidal mixing over the seamounts in the central SCS Basin plays an important role in the formation of the three separated subbasin-scale cyclonic eddies.

d. Meridional overturning circulation

The MOC in the SCS Basin is examined by the meridional streamfunction, which is defined by

$$\psi(y,z) = \int_{x_w}^{x_e} dx \int_{-H}^{z} v\, dz, \tag{6}$$

where $\psi(y, z)$ is the meridional streamfunction, v is the velocity in the y direction, and x_w and x_e denote the western and eastern boundaries, respectively.

Considering the presence of both source and sink in the open LS, the SCS MOC south of 18.5°N is shown in Fig. 10, with negative and positive streamlines corresponding to clockwise and counterclockwise circulations, respectively. There is a clockwise vertical cell in the upper layer for all experiments, which appears to be quite weakly influenced by tidal mixing. However, the MOC in the mid- and deep layers are both quite sensitive to the tidal mixing, as discussed below.

The distinct feature of the MOC in experiments TM-SCS (Fig. 10c) and TM-SCSLS (Fig. 10d) is the sandwich pattern, which is consistent with the three layers of the LS transport. A relatively strong clockwise MOC is found in the upper layer above 300-m depth, which indicates that the upper inflow water from the LS sinks in the northern SCS and gradually upwells from north to south. A quite weak counterclockwise MOC appears between 300- and 1000-m depths, indicating a northward transport in the midlayer. The deep MOC is clockwise below 1000-m depth with extremely intensive streamlines in the northern side and slight enhancement for TM-SCSLS around 2000-m depth, which indicates that the deep inflow water from the LS sharply falls into the northern SCS deep basin and eventually upwells in the southern SCS. This basin-scale sandwich structure of the SCS MOC in experiments TM-SCS and TM-SCSLS

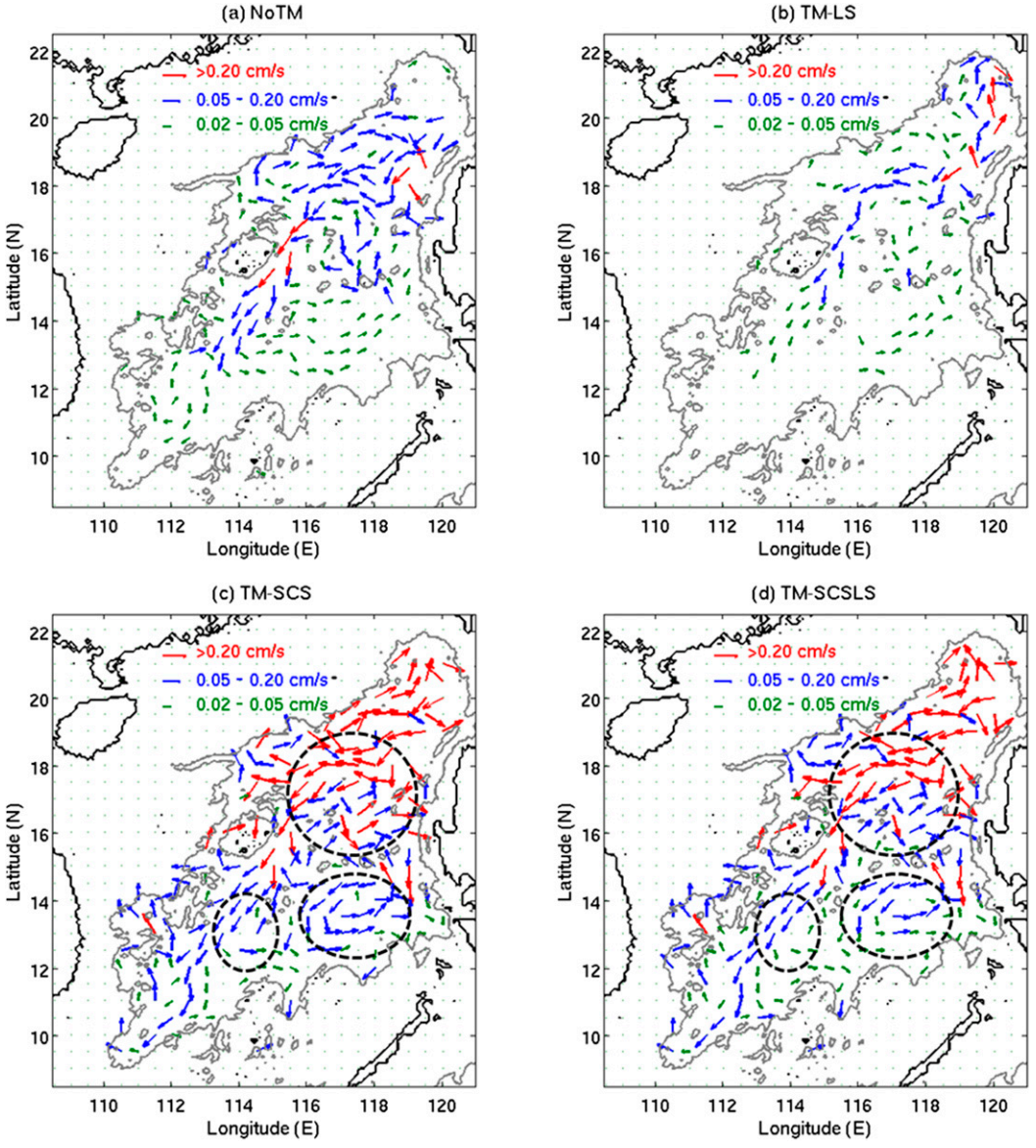

FIG. 9. Vertical-averaged currents from 2400 m to the bottom in the SCS Basin for the experiment (a) NoTM, (b) TM-LS, (c) TM-SCS, and (d) TM-SCSLS. The velocity vectors are scaled into three categories with speeds of 0.02–0.05 m s^{-1} (green arrows), 0.05–0.20 m s^{-1} (blue arrows), and >0.20 m s^{-1} (red arrows), respectively. The three black dashed circles in (c) and (d) indicate the three subbasin-scale cyclonic eddies. The gray contours represent the 2400-m isobaths.

is consistent with the previous study using the high-resolution global reanalysis data (Shu et al. 2014), although with some subbasin-scale discrepancies and relatively weaker strength. In contrast, the deep SCS MOC is significantly weaker in experiment TM-NoTM (Fig. 10a) and even disappears in experiment TM-NoTM (Fig. 10b). These results indicate that tidal mixing in the SCS could induce more vigorous meridional overturning circulation and upward water transport in the abyssal SCS Basin, whereas tidal mixing in the LS would weaken these processes.

5. Conclusions and discussion

In this paper, the impact of tidal mixing on the water mass transformation and circulation in the SCS is investigated through a set of numerical experiments. This is realized by applying different configurations of diapycnal diffusivity in a high-resolution regional model. Our key finding is that tidal mixing in both the LS and the SCS is essential for sustaining a continuous density gradient and thus a persistent outward-directed baroclinic pressure gradient across the LS, so as to maintain

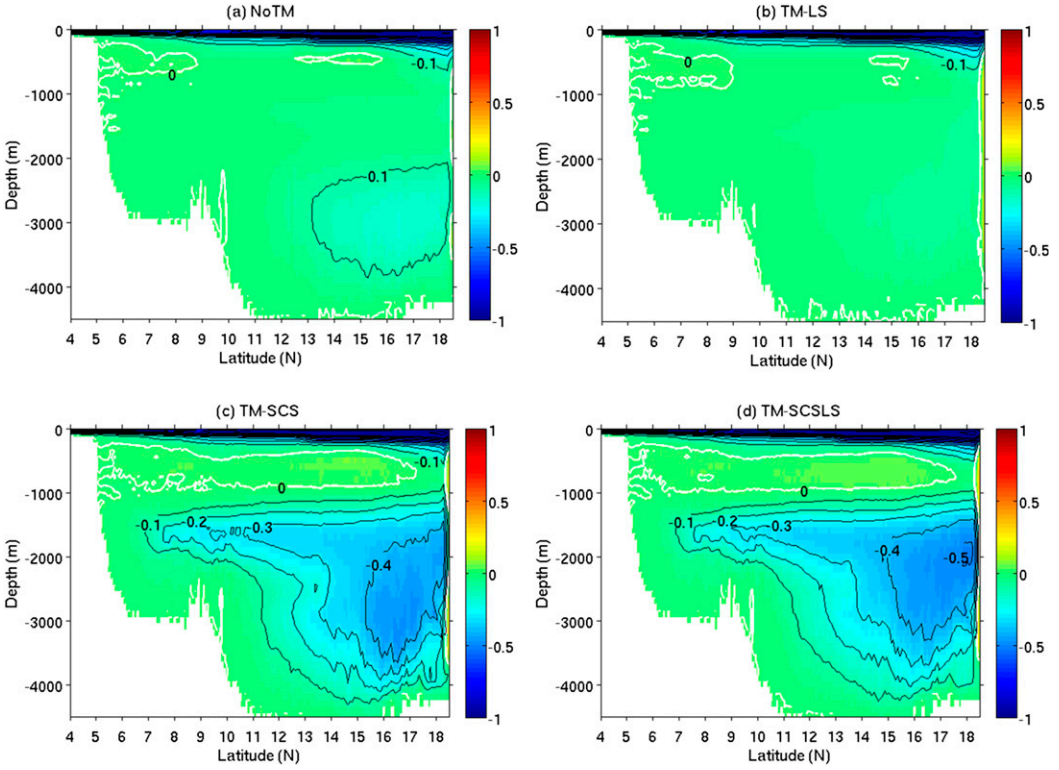

FIG. 10. Meridional overturning streamfunctions (Sv) in the SCS Basin for the experiment (a) NoTM, (b) TM-LS, (c) TM-SCS, and (d) TM-SCSLS. Negative and positive streamlines correspond to clockwise and counterclockwise circulations, respectively.

the strong deep-water transport through the LS. Nevertheless, in terms of the individual role of the tidal mixing in the LS or the SCS, it is found that tidal mixing in the deep LS would weaken the horizontal density gradient in the SCS deep basin and thus the deep SCS currents; in contrast, tidal mixing in the deep SCS would strengthen the horizontal density gradient in the SCS deep basin and thus intensify the horizontal basin-scale cyclonic circulation and the overturning circulation as well as generate the subbasin-scale abyssal eddies. Moreover, our results indicate that the tide-induced diapycnal mixing in the LS or/and SCS significantly speeds up the deep-water renewal in the SCS Basin, which makes the model spinup achieve an equilibrium state for the deep SCS in a relatively short time. The simulation with tidal mixing in both the LS and the SCS shows a good agreement with the previous studies, demonstrating the vitally important dynamic role of tidal mixing in controlling the water mass properties and circulation structures in the SCS.

It should be pointed out that the present study is by no means conclusive in understanding the impact of tidal mixing on the ocean state in the SCS, and several uncertainties remain. First, our current understanding on the spatial patterns of mixing processes in the LS and SCS remains rather rudimentary. Moreover, for understanding and predicting changes in the ocean state, and hence the climate system, it is necessary to embed a tidal mixing parameterization into ocean circulation models, in which the diapycnal diffusivities evolve both spatially and temporally with the model state. Many complicated physical and dynamic processes involved, such as the connection between circulation, wind forcing, mixing, and bottom topography, have not been established and are interesting topics for future studies.

Acknowledgments. This work was jointly supported by the Strategic Priority Research Program of the Chinese Academy of Sciences (XDA11010304, XDA11010204), the MOST of China (2014CB953904), and National Natural Science Foundation of China (41376021, 41676016, 41521005). ZL's participation of this work was supported by the National Natural Science Foundation of China (41622601, 41476006), the Natural Science Foundation of Fujian Province of China (2015J06010), and the National Basic Research Program of China (2012CB417402). The authors gratefully acknowledge the use of the HPCC at the South China Sea Institute of Oceanology, Chinese Academy of Sciences.

REFERENCES

Alford, M. H., M. F. Cronin, and J. M. Klymak, 2012: Annual cycle and depth penetration of wind-generated near-inertial internal waves at Ocean Station Papa in the northeast Pacific. *J. Phys. Oceanogr.*, **42**, 889–909, doi:10.1175/JPO-D-11-092.1.

——, and Coauthors, 2015: The formation and fate of internal waves in the South China Sea. *Nature*, **521**, 65–69, doi:10.1038/nature14399.

Atlas, R., R. N. Hoffman, J. Ardizzone, S. M. Leidner, J. C. Jusem, D. K. Smith, and D. Gombos, 2011: A cross-calibrated, multiplatform ocean surface wind velocity product for meteorological and oceanographic applications. *Bull. Amer. Meteor. Soc.*, **92**, 157–174, doi:10.1175/2010BAMS2946.1.

Bryan, K., and L. J. Lewis, 1979: A water mass model of the world ocean. *J. Geophys. Res.*, **84**, 2503–2517, doi:10.1029/JC084iC05p02503.

Carter, G. S., and M. C. Gregg, 2002: Intense variable mixing near the head of Monterey Submarine Canyon. *J. Phys. Oceanogr.*, **32**, 3145–3165, doi:10.1175/1520-0485(2002)032<3145:IVMNTH>2.0.CO;2.

Chang, Y. T., W. L. Hsu, J. H. Tai, T. Y. Tang, M. H. Chang, and S. Y. Chao, 2010: Cold deep water in the South China Sea. *J. Oceanogr.*, **66**, 183–190, doi:10.1007/s10872-010-0016-x.

Chao, S. Y., P. T. Shaw, and S. Y. Wu, 1996: Deep water ventilation in the South China Sea. *Deep-Sea Res. I*, **43**, 445–466, doi:10.1016/0967-0637(96)00025-8.

Chen, C.-T., and M. H. Huang, 1996: A mid-depth front separating the South China Sea Water and the Philippine Sea Water. *J. Oceanogr.*, **52**, 17–25, doi:10.1007/BF02236530.

Chu, P. C., and R. Li, 2000: South China Sea isopycnal-surface circulation. *J. Phys. Oceanogr.*, **30**, 2419–2438, doi:10.1175/1520-0485(2000)030<2419:SCSISC>2.0.CO;2.

——, N. L. Edmons, and C. W. Fan, 1999: Dynamical mechanisms for the South China Sea seasonal circulation and thermohaline variabilities. *J. Phys. Oceanogr.*, **29**, 2971–2989, doi:10.1175/1520-0485(1999)029<2971:DMFTSC>2.0.CO;2.

Egbert, G. D., and R. D. Ray, 2000: Significant dissipation of tidal energy in the deep ocean inferred from satellite altimeter data. *Nature*, **405**, 775–778, doi:10.1038/35015531.

Fang, G., Y. Wang, Z. Wei, Y. Fang, F. Qiao, and X. Hu, 2009: Interocean circulation and heat and freshwater budgets of the South China Sea based on a numerical model. *Dyn. Atmos. Oceans*, **47**, 55–72, doi:10.1016/j.dynatmoce.2008.09.003.

Gan, J., Z. Liu, and C. Hui, 2016: A three-layer alternating spinning circulation in the South China Sea. *J. Phys. Oceanogr.*, **46**, 2309–2315, doi:10.1175/JPO-D-16-0044.1.

Gent, P. R., and J. C. McWilliams, 1990: Isopycnal mixing in ocean circulation models. *J. Phys. Oceanogr.*, **20**, 150–155, doi:10.1175/1520-0485(1990)020<0150:IMIOCM>2.0.CO;2.

——, J. Willebrand, T. J. McDougall, and J. C. McWilliams, 1995: Parameterizing eddy-induced tracer transports in ocean circulation models. *J. Phys. Oceanogr.*, **25**, 463–474, doi:10.1175/1520-0485(1995)025<0463:PEITTI>2.0.CO;2.

Huang, R. X., 1999: Mixing and energetics of the oceanic thermohaline circulation. *J. Phys. Oceanogr.*, **29**, 727–746, doi:10.1175/1520-0485(1999)029<0727:MAEOTO>2.0.CO;2.

——, and X. Jin, 2002: Deep circulation in the South Atlantic induced by bottom-intensified mixing over the midocean ridge. *J. Phys. Oceanogr.*, **32**, 1150–1164, doi:10.1175/1520-0485(2002)032<1150:DCITSA>2.0.CO;2.

Jayne, S. R., 2009: The impact of abyssal mixing parameterizations in an ocean general circulation model. *J. Phys. Oceanogr.*, **39**, 1756–1775, doi:10.1175/2009JPO4085.1.

——, and L. C. St. Laurent, 2001: Parameterizing tidal dissipation over rough topography. *Geophys. Res. Lett.*, **28**, 811–814, doi:10.1029/2000GL012044.

Koch-Larrouy, A., G. Madec, P. Bouruet-Aubertot, T. Gerkema, L. Bessieres, and R. Molcard, 2007: On the transformation of Pacific Water into Indonesian Throughflow Water by internal tidal mixing. *Geophys. Res. Lett.*, **34**, L04604, doi:10.1029/2006GL028405.

——, ——, B. Blanke, and R. Molcard, 2008a: Water mass transformation along the Indonesian Throughflow in an OGCM. *Ocean Dyn.*, **58**, 289–309, doi:10.1007/s10236-008-0155-4.

——, ——, D. Iudicone, A. Atmadipoera, and R. Molcard, 2008b: Physical processes contributing to the water mass transformation of the Indonesian Throughflow. *Ocean Dyn.*, **58**, 275–288, doi:10.1007/s10236-008-0154-5.

Lan, J., N. Zhang, and Y. Wang, 2013: On the dynamics of the South China Sea deep circulation. *J. Geophys. Res. Oceans*, **118**, 1206–1210, doi:10.1002/jgrc.20104.

——, Y. Wang, F. Cui, and N. Zhang, 2015: Seasonal variation in the South China Sea deep circulation. *J. Geophys. Res. Oceans*, **120**, 1682–1690, doi:10.1002/2014JC010413.

Large, W. G., J. C. McWilliams, and S. C. Doney, 1994: Oceanic vertical mixing: A review and a model with a nonlocal boundary layer parameterization. *Rev. Geophys.*, **32**, 363–403, doi:10.1029/94RG01872.

Ledwell, J. R., A. J. Watson, and C. S. Law, 1993: Evidence for slow mixing across the pycnocline from an open-ocean tracer release experiment. *Nature*, **364**, 701–703, doi:10.1038/364701a0.

——, E. T. Montgomery, K. L. Polzin, L. C. St. Laurent, R. W. Schmitt, and J. M. Toole, 2000: Evidence of enhanced mixing over rough topography in the abyssal ocean. *Nature*, **403**, 179–182, doi:10.1038/35003164.

Li, L., and T. Qu, 2006: Thermohaline circulation in the deep South China Sea Basin inferred from oxygen distributions. *J. Geophys. Res.*, **111**, C05017, doi:10.1029/2005JC003203.

Liu, C. T., and R. J. Liu, 1988: The deep current in the Bashi Channel. *Acta Oceanogr. Taiwan.*, **20**, 107–116.

Liu, Q., H. Yang, and Z. Liu, 2001: Seasonal features of the Sverdrup circulation in the South China Sea. *Prog. Nat. Sci.*, **11**, 202–206.

Liu, Z., and I. Lozovatsky, 2012: Upper pycnocline turbulence in the northern South China Sea. *Chin. Sci. Bull.*, **57**, 2302–2306, doi:10.1007/s11434-012-5137-8.

Lozovatsky, I., Z. Liu, H. J. S. Fernando, J. Hu, and H. Wei, 2013: The TKE dissipation rate in the northern South China Sea. *Ocean Dyn.*, **63**, 1189–1201, doi:10.1007/s10236-013-0656-7.

Ma, B. B., R. C. Lien, and D. S. Ko, 2013: The variability of internal tides in the northern South China Sea. *J. Oceanogr.*, **69**, 619–630, doi:10.1007/s10872-013-0198-0.

MacKinnon, J., 2013: Mountain waves in the deep ocean. *Nature*, **501**, 321–322, doi:10.1038/501321a.

——, and M. C. Gregg, 2003: Mixing on the late summer New England shelf—Solibores, shear, and stratification. *J. Phys. Oceanogr.*, **33**, 1476–1492, doi:10.1175/1520-0485(2003)033<1476:MOTLNE>2.0.CO;2.

Mantyla, A. W., 1975: On the potential temperature in the abyssal Pacific Ocean. *J. Mar. Res.*, **33**, 341–354.

Marshall, J., and K. G. Speer, 2012: Closure of the meridional overturning circulation through Southern Ocean upwelling. *Nat. Geosci.*, **5**, 171–180, doi:10.1038/ngeo1391.

——, A. Adcroft, C. Hill, L. Perelman, and C. Heisey, 1997: A finite-volume, incompressible Navier Stokes model for studies of the ocean on parallel computers. *J. Geophys. Res.*, **102**, 5753–5766, doi:10.1029/96JC02775.

Melet, A., R. W. Hallberg, S. Legg, and K. Polzin, 2013: Sensitivity of the ocean state to the vertical distribution of internal-tide-driven mixing. *J. Phys. Oceanogr.*, **43**, 602–615, doi:10.1175/JPO-D-12-055.1.

Munk, W., and C. Wunsch, 1998: Abyssal recipes II: Energetics of tidal and wind mixing. *Deep-Sea Res. I*, **45**, 1977–2010, doi:10.1016/S0967-0637(98)00070-3.

Nikurashin, M., and R. Ferrari, 2013: Overturning circulation driven by breaking internal waves in the deep ocean. *Geophys. Res. Lett.*, **40**, 3133–3137, doi:10.1002/grl.50542.

Niwa, Y., and T. Hibiya, 2014: Generation of baroclinic tide energy in a global three-dimensional numerical model with different spatial grid resolutions. *Ocean Modell.*, **80**, 59–73, doi:10.1016/j.ocemod.2014.05.003.

Osborn, T. R., 1980: Estimates of the local rate of vertical diffusion from dissipation measurements. *J. Phys. Oceanogr.*, **10**, 83–89, doi:10.1175/1520-0485(1980)010<0083:EOTLRO>2.0.CO;2.

Polzin, K. L., 2009: An abyssal recipe. *Ocean Modell.*, **30**, 298–309, doi:10.1016/j.ocemod.2009.07.006.

——, J. M. Toole, J. R. Ledwell, and R. W. Schmitt, 1997: Spatial variability of turbulent mixing in the abyssal ocean. *Science*, **276**, 93–96, doi:10.1126/science.276.5309.93.

Qu, T. D., 2000: Upper-layer circulation in the South China Sea. *J. Phys. Oceanogr.*, **30**, 1450–1460, doi:10.1175/1520-0485(2000)030<1450:ULCITS>2.0.CO;2.

——, 2002: Evidence for water exchange between the South China Sea and the Pacific Ocean through the Luzon Strait. *Acta Oceanol. Sin.*, **21**, 175–185.

——, J. B. Girton, and J. A. Whitehead, 2006: Deepwater overflow through Luzon Strait. *J. Geophys. Res.*, **111**, C01002, doi:10.1029/2005JC003139.

——, T. Song, and T. Yamagata, 2009: An introduction to the South China Sea throughflow: Its dynamics, variability, and implication for climate. *Dyn. Atmos. Oceans*, **47**, 3–14, doi:10.1016/j.dynatmoce.2008.05.001.

Redi, M. H., 1982: Oceanic isopycnal mixing by coordinate rotation. *J. Phys. Oceanogr.*, **12**, 1154–1158, doi:10.1175/1520-0485(1982)012<1154:OIMBCR>2.0.CO;2.

Saenko, O. A., and W. J. Merryfield, 2005: On the effect of topographically enhanced mixing on the global ocean circulation. *J. Phys. Oceanogr.*, **35**, 826–834, doi:10.1175/JPO2722.1.

Scott, R. B., J. A. Goff, A. C. Naveira Garabato, and A. J. Nurser, 2011: Global rate and spectral characteristics of internal gravity wave generation by geostrophic flow over topography. *J. Geophys. Res.*, **116**, C09029, doi:10.1029/2011JC007005.

Shaw, P. T., and L. Fu, 1999: Sea surface height variations in the South China Sea from satellite altimetry. *Oceanol. Acta*, **22**, 1–17, doi:10.1016/S0399-1784(99)80028-0.

Shu, Y., H. Xue, D. Wang, F. Chai, Q. Xie, J. Yao, and J. Xiao, 2014: Meridional overturning circulation in the South China Sea envisioned from the high-resolution global reanalysis data GLBa0.08. *J. Geophys. Res. Oceans*, **119**, 3012–3028, doi:10.1002/2013JC009583.

Simmons, H. L., S. R. Jayne, L. C. St. Laurent, and A. J. Weaver, 2004: Tidally driven mixing in a numerical model of the ocean general circulation. *Ocean Modell.*, **6**, 245–263, doi:10.1016/S1463-5003(03)00011-8.

Smagorinsky, J., 1993: Large eddy simulation of complex engineering and geophysical flows. *Evolution of Physical Oceanography*, B. Galperin and S. A. Orszag, Eds., Cambridge University Press, 3–36.

St. Laurent, L. C., 2008: Turbulent dissipation on the margins of the South China Sea. *Geophys. Res. Lett.*, **35**, L23615, doi:10.1029/2008GL035520.

——, H. L. Simmons, and S. R. Jayne, 2002: Estimating tidally driven mixing in the deep ocean. *Geophys. Res. Lett.*, **29**, 2106, doi:10.1029/2002GL015633.

——, ——, T. Y. Tang, and Y. H. Wang, 2011: Turbulent properties of internal waves in the South China Sea. *Oceanography*, **24**, 78–87, doi:10.5670/oceanog.2011.96.

Talley, L. D., 2013: Closure of the global overturning circulation through the Indian, Pacific, and Southern Oceans: Schematics and transports. *Oceanography*, **26**, 80–97, doi:10.5670/oceanog.2013.07.

Tian, J., Q. Yang, X. Liang, L. Xie, D. Hu, F. Wang, and T. Qu, 2006: Observation of Luzon Strait transport. *Geophys. Res. Lett.*, **33**, L19607, doi:10.1029/2006GL026272.

——, ——, and W. Zhao, 2009: Enhanced diapycnal mixing in the South China Sea. *J. Phys. Oceanogr.*, **39**, 3191–3203, doi:10.1175/2009JPO3899.1.

Wang, G. H., S. P. Xie, T. D. Xie, and R. X. Huang, 2011: Deep South China Sea circulation. *Geophys. Res. Lett.*, **38**, L05601, doi:10.1029/2010GL046626.

Wang, J., 1986: Observation of abyssal flows in the northern South China Sea. *Acta Oceanogr. Taiwan*, **16**, 36–45.

Wang, X., S. Peng, Z. Liu, R. X. Huang, Y. K. Qian, and Y. Li, 2016: Tidal mixing in the South China Sea: An estimate based on the internal tide energetics. *J. Phys. Oceanogr.*, **46**, 107–124, doi:10.1175/JPO-D-15-0082.1.

Wu, L., Z. Jing, S. Riser, and M. Visbeck, 2011: Seasonal and spatial variations of Southern Ocean diapycnal mixing from Argo profiling floats. *Nat. Geosci.*, **4**, 363–366, doi:10.1038/ngeo1156.

Wunsch, C., and R. Ferrari, 2004: Vertical mixing, energy, and the general circulation of the oceans. *Annu. Rev. Fluid Mech.*, **36**, 281–314, doi:10.1146/annurev.fluid.36.050802.122121.

Wyrtki, K., 1961: *Physical Oceanography of the Southeast Asian Waters*. NAGA Rep., Vol. 2, Scripps Institute of Oceanography, 195 pp.

Xie, Q., J. Xiao, D. Wang, and Y. Yu, 2013: Analysis of deep-layer and bottom circulations in the South China Sea based on eight quasi-global ocean model outputs. *Chin. Sci. Bull.*, **58**, 4000–4011, doi:10.1007/s11434-013-5791-5.

Xue, H., F. Chai, N. Pettigrew, D. Xu, M. Shi, and J. Xu, 2004: Kuroshio intrusion and the circulation in the South China Sea. *J. Geophys. Res.*, **109**, C02017, doi:10.1029/2002JC001724.

Yang, Q., J. Tian, and W. Zhao, 2010: Observation of Luzon Strait transport in summer 2007. *Deep-Sea Res. I*, **57**, 670–676, doi:10.1016/j.dsr.2010.02.004.

——, ——, ——, X. Liang, and L. Zhou, 2014: Observations of turbulence on the shelf and slope of northern South China Sea. *Deep-Sea Res. I*, **87**, 43–52, doi:10.1016/j.dsr.2014.02.006.

——, W. Zhao, X. Liang, and J. Tian, 2016: Three-Dimensional distribution of turbulent mixing in the South China Sea. *J. Phys. Oceanogr.*, **46**, 769–788, doi:10.1175/JPO-D-14-0220.1.

Yaremchuk, M., J. McCreary Jr., Z. Yu, and R. Furue, 2009: The South China Sea throughflow retrieved from climatological data. *J. Phys. Oceanogr.*, **39**, 753–767, doi:10.1175/2008JPO3955.1.

Yuan, D., 2002: A numerical study of the South China Sea deep circulation and its relation to the Luzon Strait transport. *Acta Oceanol. Sin.*, **21**, 187–202.

Zhao, W., C. Zhou, J. Tian, Q. Yang, B. Wang, L. Xie, and T. Qu, 2014: Deep water circulation in the Luzon Strait. *J. Geophys. Res. Oceans*, **119**, 790–804, doi:10.1002/2013JC009587.

Zhao, Z., 2014: Internal tide radiation from the Luzon Strait. *J. Geophys. Res. Oceans*, **119**, 5434–5448, doi:10.1002/2014JC010014.

Zhou, C., W. Zhao, J. Tian, Q. Yang, and T. Qu, 2014: Temporal variability of the deep circulation in the Luzon Strait. *J. Phys. Oceanogr.*, **44**, 2972–2986, doi:10.1175/JPO-D-14-0113.1.